

Exchange-Correlation Effect in the Charge Response of a Warm Dense Electron Gas

Peng-Cheng Hou¹, Bao-Zong Wang¹, Kristjan Haule⁴, Youjin Deng^{1,2,3}, and Kun Chen^{5*}

¹ *Department of Modern Physics, University of Science and Technology of China, Hefei, Anhui 230026, China*

² *Hefei National Laboratory, University of Science and Technology of China, Hefei 230088, China*

³ *MinJiang Collaborative Center for Theoretical Physics,*

College of Physics and Electronic Information Engineering, Minjiang University, Fuzhou 350108, China

⁴ *Department of Physics and Astronomy, Rutgers,*

The State University of New Jersey, Piscataway, New Jersey 08854-8019 USA and

⁵ *Center for Computational Quantum Physics, Flatiron Institute, 162 5th Avenue, New York, New York 10010. The Flatiron Institute is a division of the Simons Foundation*

(Dated: September 19, 2022)

The study of warm dense matter, widely existing in nature and laboratories, is challenging due to the interplay of quantum and classical fluctuations. We develop a variational diagrammatic Monte Carlo method and determine the exchange-correlation kernel $K_{xc}(q; T)$ of a warm dense electron gas for a broad range of temperature T and momentum q . We observe several interesting physics, including the T -dependent evolution of the hump structure and the large- q tail and the emergence of a scaling relation. Particularly, by deriving an analytical form for $q \rightarrow \infty$, we obtain large- q tails of K_{xc} with high precision. It is shown that the K_{xc} data can be reliably transformed into real space, which can be directly used in density-functional-theory calculations of real warm dense matter.

Over the past two decades, extensive research interests have been devoted to an extreme state of matter at high temperature and density, called warm dense matter (WDM). The WDM region occurs in various astrophysical objects such as giant planet interiors [1–5], brown dwarfs [6, 7], and neutron crusts [8]. Nowadays, it can be routinely realized and probed in novel high-power laser and accelerator facilities [9–12]. The electrons in WDM are about to lose quantum coherence while still demonstrating nontrivial quantum corrections, resulting in a special crossover state between classical plasma and quantum condensed matter.

Within the local-density approximation treatment, the electrons in WDM are modeled by the warm dense uniform electron gas (UEG). The UEG only has two parameters, the density parameter (Wigner-Seitz radius) $r_s = \bar{r}/a_B$ and the reduced temperature $\theta = T/T_F$, where \bar{r} is the average interparticle distance, a_B is Bohr radius, and T_F is the Fermi temperature. At the high-density limit ($r_s \rightarrow 0$), the electrons behave as an ideal Fermi gas; at low density, the Coulomb potential becomes dominant, eventually resulting in a Wigner crystal [13–15]. Dimensional temperature ratio θ can be seen as a quantum degeneracy parameter. In the high-temperature ($\theta \gg 1$) and zero-temperature ($\theta \rightarrow 0$) limits, the UEG has been well described by the classical plasma theory and the quantum condensed matter theory, respectively. However, due to the complicated interplay of electronic correlations, quantum coherence, and thermal fluctuations, the crossover regime $r_s \sim \theta \sim 1$, particularly relevant for WDM, is much less understood.

The density (or charge) response function, one of the most important electronic probes, is measured in many vital diagnostic experiments of WDM [16–21]. The random phase approximation (RPA) well describes the long-range screening effects and is a reasonable approximation

in the weakly interacting regimes. However, it becomes invalid in the WDM conditions because the RPA response function only accounts for the Hartree component of the induced potentials [22] and overestimates the short-range correlations between electrons. The neglected exchange-correlation (XC) component can be parameterized by the local field correction (LFC),

$$G(q, \omega) = 1 - \frac{1}{v_q} \left[\frac{1}{\chi_0(q, \omega)} - \frac{1}{\chi(q, \omega)} \right], \quad (1)$$

where $\chi_0(q, \omega)$ and $\chi(q, \omega)$ are the dynamic density response functions of noninteracting and interacting systems, respectively, and $v_q = 8\pi/q^2$ is the long-range Coulomb repulsion (Rydberg atomic units are used). The LFC encodes the structure of effective electron-electron interaction and is crucial for the understanding of many experimental phenomena, exemplified by plasmon [11, 23], Coulomb and spin-Coulomb drag effects [24, 25], electrical and thermal conductivities [26, 27], stopping power [28, 29], and energy transfer rates [30]. In the time-dependent density functional theory (TDDFT) [22, 31, 32], the so-called XC kernel, $K_{xc}(q, \omega) = -v_q G(q, \omega)$, is typically used as an input for *ab-initio* calculations of ground-state energies and electronic spectra in real materials. For small- and large- q , since $G(q) \propto q^2$, the behavior of G is better described by K_{xc} .

Substantial efforts have been devoted to studying the LFC of UEG, particularly its static one $G(q) \equiv G(q, \omega = 0)$. At $T = 0$, in the ground state, analytic properties of the LFC in the small- and large- q limits were derived [33–36] and numerical calculations of $G(q)$ were performed for various density parameters by diffusion quantum Monte Carlo [37, 38]. Recently, Chen and Haule developed a variational diagrammatic Monte Carlo (VDMC) method [39] using renormalized Feynman diagrammatic expansion and used it to obtain accurate re-

sults on the static density LFC [39] and spin LFC [40] for $r_s \leq 5$. Furthermore, the dynamic LFC was computed by implementing the algorithmic Matsubara integration with the VDMC [41]. For finite T , calculations of $G(q)$ are amenable due to the recent development of unbiased path-integral Monte Carlo (PIMC) methods [42–45]. Dornheim *et al.* [46] reported a neural-network representation of $G(q)$ based on PIMC data and ground-state parametrization [47]. They further gave an analytic parametrization of $G(q)$ within effective static approximation [48] and used it to describe the response functions in the WDM regime [49, 50].

Many challenges still exist. First, due to the limited precision of ground-state data, it remains controversial whether the LFC develops a peak structure near $q = 2k_F$ (where k_F is the Fermi momentum), termed the “ $2k_F$ hump puzzle” [51]. Second, the PIMC methods suffer from the notorious sign problem [52–54] as the electrons become a degenerate quantum liquid for $T < T_F$ [55]. Therefore, our current knowledge has a significant gap: how the LFC evolves from zero T in the ground state, via low T relevant for condensed matter physics and intermediate T corresponding to WDM, and finally to high T relevant for classical plasma. Third, the PIMC extracts $G(q)$ from $\chi(q)$ via (1), but it is difficult to determine the large- q LFC because statistical errors in MC data can easily overwhelm the very weak many-body contribution to $\chi(q) - \chi_0(q)$ for $q > 3k_F$. To develop an efficient algorithm for large q , it is desirable to analytically derive the asymptotic properties of $G(q)$ in the large- q limit. In application, this is particularly important since many TDDFT algorithms require an XC kernel $K_{xc}(r)$ in real space, and, without accurate data for large q and analytical forms for $q \rightarrow \infty$, a reliable Fourier transform from $K_{xc}(q)$ to $K_{xc}(r)$ is extremely difficult due to the Gibbs phenomenon.

In this letter, we develop the VDMC method for the warm dense electron gas, which is a generalization of the method introduced by two of us [39]. Inspired by the binary expression tree in computer science, we introduce an expression tree representation of Feynman diagrams to efficiently and accurately calculate $\chi(q)$. Our VDMC method is reliable for the UEG of high to intermediate density and at arbitrary temperature, covering those low- T and large- q regimes where other unbiased finite- T quantum MC methods are infeasible. From extensive simulations, we obtain high-precision data of the static LFC in a broad range of (q, T) space from the Fermi liquid to WDM and then to classical plasma. Several interesting physics are revealed, including the T -dependent evolution of the hump structure and the large- q tail (Fig. 1) and the emergence of an asymptotic high- T scaling relation of $G(q; r_s, T)$ (we use a semicolon to separate intrinsic variables including q , ω , and r , and parameter variables including r_s and T) in dimensionless variable q/\sqrt{T} (Fig. 2(a)). High-precision data for K_{xc}

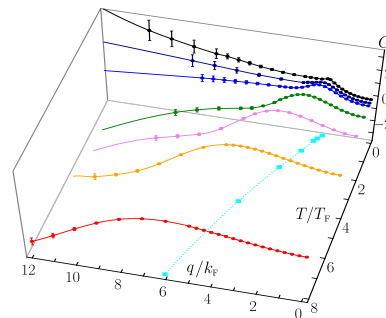


FIG. 1. Static local field correction $G(q)$ in the extensive (q, T) plane for $r_s = 1$. The circles depict VDMC data points for $\theta = 0.0625, 0.25, 0.4, 1, 2, 4, 8$. The cyan squares and dotted line depict the tendency of the maximum momentum q_{\max} of $G(q)$ versus T .

are obtained up to $14k_F$, shown in Fig. 2(b). In both the small- and the large- q limit, $K_{xc}(q)$ saturates to a constant, non-monotonically depending on T . Moreover, we show that the asymptotic XC kernel $K_\infty \equiv K_{xc}(q \rightarrow \infty)$ is proportional to the interaction-induced shift of the kinetic energy and derive the analytical form of the coefficient. Using a VDMC, we compute the kinetic energy accurately and thus K_∞ as a function of T (the inset of Fig. 2(c)). Combining data of $K_{xc}(q)$ for $q \leq 14k_F$ and of K_∞ for the tail, we show that the Fourier transform of $K_{xc}(q)$ to real space can be performed reliably without any freely adjustable parameter (Fig. 2(c)).

Results - We carry out extensive simulations for the three-dimensional UEG model at a series of temperatures $\theta = 0.0625, 0.25, 0.4, 1, 2, 4, 8$. Hereby, we focus on parameter $r_s = 1$, which is the most typical WDM density, and we also simulate $r_s = 2$ for $\theta = 4, 8$ to illustrate the r_s -independent scaling relation. We accurately determine the static LFC $G(q; T)$ up to $q/k_F = 14$ (Fig. 1), more than four times larger than the previous studies [46, 58]. Accordingly, the XC kernel $K_{xc}(q; T)$ is obtained in Fig. 2(b).

Our data exhibit several profound features of the T - and q -resolved LFC. For any given T , there is a unique momentum q_{\max} corresponding to the local peak in $G(q)$, which separates long-range (small- q) from short-range (large- q) physics. Figure 1 shows that the peak broadens and shifts to the larger momentum as T increases, and the inset of Fig. 2(a) shows q_{\max} as a function of T . In the high- T limit, q_{\max} is controlled by the thermal de Broglie wavelength $\lambda_{th} = \sqrt{4\pi/T}$ as $q_{\max} \approx 7.6\lambda_{th}^{-1}$. As T decreases, the value of q_{\max} gradually decreases and is no longer dominated by λ_{th} for $T \lesssim 2T_F$, eventually converging to $\simeq 2k_F$ at zero T . We further observe that in the evolution of the XC kernel $K_{xc}(q)$ with T (Fig. 2(b)), a local minimum appears at $T \lesssim 0.4T_F$ and becomes sharper and closer to $q \simeq 2k_F$ as $T \rightarrow 0$. These numerical results confirm the “ $2k_F$ hump” of the

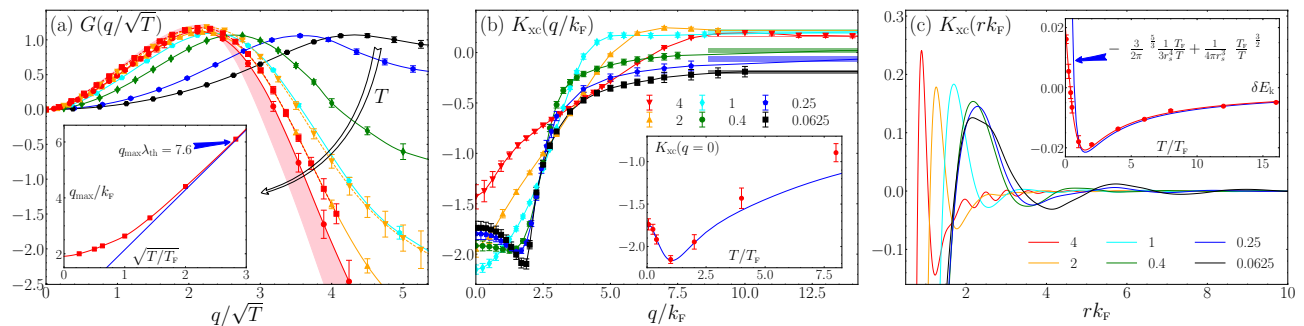


FIG. 2. (a) Rescaled static LFC as a function of q/\sqrt{T} . The data points with solid lines are for $r_s = 1$ and $\theta = 0.25, 0.4, 1, 2, 4, 8$, and ones with dashed lines are for $r_s = 2$ and $\theta = 4, 8$. As $T \rightarrow \infty$, the LFC data tend to collapse to a universal curve that depends on q/\sqrt{T} , and is covered in the pink shadow. The inset shows the evolution of q_{\max} from $\simeq 2k_F$ in the zero- T limit to $\approx 7.6\lambda_{\text{th}}$ in the high- T limit. (b) The XC kernel $K_{\text{xc}}(q)$ for different temperatures and $r_s = 1$. The tail of either curve converges to a constant K_∞ that is explicitly calculated by the VDMC as Eq.(3), and the strip marks its value and error. The inset shows the evolution of $K_{\text{xc}}(q=0, T)$. Our data are consistent with the parameterized function [56] (blue line). (c) The XC kernel of UEG in real space with the delta-peaked term subtracted. The inset shows the interaction-induced shift of the kinetic energy versus temperature. Our data is approaching the high- T approximation [57] (blue line) for $\theta > 1$.

ground-state UEG postulated in various theoretical predictions [59–62]. Moreover, the nontrivial T -dependence of q_{\max} and the smearing out of the sharp minimum in K_{xc} at $T \sim T_F$ reflect the intense competition between quantum and thermal fluctuations in the WDM regime.

In addition, with increasing T , the large- q LFC evolves from a positive tail at low T to a negative tail for $T \gtrsim 0.4T_F$. Holas [35] predicted the asymptotic behavior $G(q) \propto q^2$ for $q \rightarrow \infty$ at zero T , where the prefactor is proportional to the change in the interaction-induced shift of the kinetic energy δE_k and is positive for all r_s . However, no analytical formula currently exists for finite T . Qualitatively, the evolution of the LFC tail reflects the sophisticated competition of Coulomb repulsion, exchange effects, and thermal motion.

We argue that in the high- T limit, the entire LFC curve is described by an asymptotic scaling function depending on a single dimensionless parameter q/\sqrt{T} , independent of r_s , as

$$\lim_{T \rightarrow \infty} |_{\text{fixed } \alpha} G(q; r_s, T) = \tilde{G}(\alpha) \quad \alpha = q/\sqrt{T}. \quad (2)$$

The argument is as follows: for UEG, there are two characteristic length scales, i.e., λ_{th} and r_s . When $T \rightarrow \infty$, the only detectable length scale is λ_{th} since $\lambda_{\text{th}} \ll r_s$. Indeed, Figure 2(a) demonstrates that as T increases, the LFC tends to collapse into a universal curve as Eq. 2.

We now turn to the XC kernel. Figure 2(b) shows that $K_{\text{xc}}(q)$ converges to a nonmonotonic T -dependent constant for both $q \rightarrow 0$ and $q \rightarrow \infty$. It is known that the uniform XC kernel $K_{\text{xc}}(q=0)$ is proportional to the second derivative of the XC free energy, given by the compressibility sum rule [63]. Therefore, we compare our $K_{\text{xc}}(q=0)$ data with the values from the recent XC free-energy parametrization [56] in the inset of Fig. 2(b). It is shown that they are consistent for $\theta \leq 2$ within error bars while having a slight deviation for $\theta \geq 4$.

The large- q behavior of the XC kernel is highly nontrivial, as also discussed in the LFC tail. Based on the large- q expansion of the polarization function Π related to the density response function by $\chi(q, \omega) = [\Pi^{-1}(q, \omega) + v_q]^{-1}$ (details are given in the Supplementary Material [64]), we derive the asymptotic formula of the large- q XC kernel for finite T as

$$\lim_{q \rightarrow \infty} K_{\text{xc}}(q; r_s, T) = K_\infty(r_s, T) + \mathcal{O}(q^{-2}), \quad (3)$$

with $K_\infty = -(32\pi^2 r_s^6 / 27) \delta E_k$. This analytic formula generalizes the zero- T one [35] and describes that the convergent constant K_∞ is controlled by the many-body contributions of the kinetic energy. Note that Eq. 3 still holds for the dynamic XC kernel since the frequency dependence only exists in the subleading and higher orders. We explicitly calculate the kinetic energies by the VDMC to extract K_∞ for various temperatures, and the results are consistent with our large- q K_{xc} data within error bars, as shown in Fig. 2(b). Furthermore, the inset of Fig. 2(c) displays an interesting nonmonotonic behavior: as T increases, δE_k decreases from a positive value for low T to negative for $\theta \gtrsim 0.4$ and finally approaches zero asymptotically. At zero T , δE_k is always positive because electron repulsion broadens the ground-state momentum distribution. However, at high enough temperatures, the correlation effects would lead to the narrowing of the momentum distribution [57, 65, 66]; meanwhile, the Hartree-Fock term $-(3/2\pi)^{5/3} \theta / (3r_s^4)$ dominates the XC contribution to the kinetic energy so that $\delta E_k < 0$. Remarkably, we find that the high- T approximation [57], including the Hartree-Fock and the Montroll-Ward contributions, describes well the nonmonotonic T -dependence of δE_k for $\theta \geq 1$. The formula (3) combined with the behavior of δE_k versus T explains the T -dependent evolution of the LFC/XC kernel tail and matches the scaling

relation in the high- T limit.

Combining our numerical data and the analytical tail, we perform interpolation and obtain a controlled representation of the XC kernel for overall momentum (the solid line of Fig. 2(b)). In practice, we use spline interpolation to fit piecewise cubic polynomials to $q \leq q_{\text{cut}}$ data (the cutoff momentum q_{cut} excludes the tail and depends on the temperature). We then perform the least-squares fits to $q > q_{\text{cut}}$ data via the ansatz $K_{\text{xc}}(q) = K_{\infty} + a/q^2$, where K_{∞} is fixed by δE_{k} data and a is the fitting parameter. The overall $K_{\text{xc}}(q)$ enables a Fourier transform to the real-space XC kernel $K_{\text{xc}}(r)$ without relying on any ansatz of $K_{\text{xc}}(q)$. The constant tail in $K_{\text{xc}}(q)$ translates to a contact term $K_{\infty}\delta^{(3)}(r)$ in real space, while the rest part of the XC kernel transforms into a smooth function of the distance r , as shown in Fig. 2(c). This scheme allows us to accurately represent $K_{\text{xc}}(r)$, which is a key input in TDDFT calculations for real materials.

Methods - Diagrammatic expansion is used to perturbatively calculate a quantity as a series of integrals which can be visualized as Feynman diagrams. It allows us to simulate quantities immediately in the thermodynamic limit by a Markov-chain process that stochastically samples diagrams and internal variables. Such diagrammatic MC methods have found successful applications in many physical problems [67–92]. For UEG, the expansion in the bare Coulomb interaction is divergent and needs to be transformed into a more appropriate power expansion, as explained below. We use the variational scheme [39, 93], in which the emergent low-energy physics is taken into account at the lowest order, and the corrections are perturbatively added, leading to rapid convergence. We develop a VDMC method, which has a generic algorithmic structure and an optimized efficiency with the help of an expression-tree representation of diagrams.

Motivated by the Coulomb screening effects, we introduce a variational inverse screening length λ_q following Ref. [39] to re-expand the bare interaction $\frac{8\pi}{k^2} = \frac{8\pi}{k^2 + \lambda_q^2} \sum_{n=0}^{\infty} \left(\frac{\lambda_q^2}{8\pi} \frac{8\pi}{k^2 + \lambda_q^2} \right)^n$. In the VDMC, λ_q is q -dependent and optimized to achieve a rapid convergence according to the principle of minimal sensitivity [94]. To further speed up the convergence, we insert the Fock sub-diagram into the bare electron propagator to recover the screened Hartree-Fock approximation in the first order. Meanwhile, we add order-by-order chemical-potential counterterms to fix the Fermi surface at each order. Within this optimized expansion, we can obtain reliable infinite-order results of arbitrary quantities without very large truncation order N , which avoids the exponential scaling of the computation time with order. Fig. 3(a) shows the static polarization $\Pi(q)$, which rapidly converges at the optimal λ_q . In practical simulations, we choose λ_q as piecewise constants for $q \lesssim 6k_{\text{F}}$ and $q \gtrsim 6k_{\text{F}}$, which is already sufficient for rapid convergence. We compute the Feynman diagrams up to order $N = 5$,

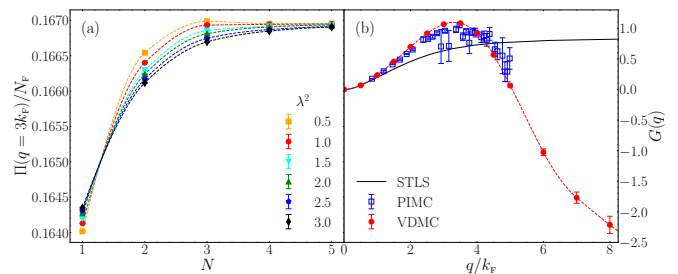


FIG. 3. (a) Static polarization scaled by the density of states at the Fermi level N_{F} at $q = 3k_{\text{F}}$ versus truncation order N for $\theta = 2$ and $r_s = 1$. All λ choices lead to the same extrapolated value, and the optimal λ for the fastest convergence is about 1.0 in this case. (b) LFC $G(q)$ at $\theta = 2$ and $r_s = 1$ for the VDMC (red circles), the PIMC [46] (blue squares), and the STLS approximation [96] (black line).

which contain about 1200 diagrams. Our calculations suggest that, at least for UEG, $N = 5$ is already sufficient for us to reliably extrapolate $\Pi(q)$ to infinite order. The description of details, including the topology and number of Feynman diagrams and numerical approach, can be found in Ref. [39].

A major challenge of the VDMC is how to generate and group a large number of Feynman diagrams and efficiently compute their weights. By sign-structure analysis of scattering amplitudes in diagrams constrained by the crossing symmetry and the conservation law [95], we can optimize the internal-variable arrangements and construct the sign-canceled diagram groups to alleviate the sign problem significantly. Inspired by the binary expression tree in data structures, we develop a universal expression tree representation of diagrams implemented by a diagram mini-compiler with a three-layer infrastructure. We are improving the original code for readability and usability and will report details elsewhere.

By the VDMC method, we obtain more accurate LFC data over a wider range of (q, T) than the state-of-the-art PIMC [46], as shown in Fig. 3(b). We note that for the LFC at large momenta, the PIMC cannot provide reliable results because the statistical errors of data of χ ($\sim 1/q^2$) overwhelm $\chi - \chi_0$ ($\sim 1/q^4$) [64]. Here, based on the large- q expansion of $\chi(q)$ [64], we identify each polarization diagram with a tail-decaying behavior $q^{-\ell}$, where ℓ is the least number of the propagator lines with flowing q . Hence, we optimally organize the external momentum variable of each diagram to make the integrand have the same tail behavior as the integral so that the VDMC can directly calculate $\chi - \chi_0$ by efficiently sampling each diagram with a reweighting factor q^{ℓ} . For completeness, we mention that a VDMC simulation for a single $r_s - \theta$ system parameter takes $O(10^4)$ CPU (single-threaded process) hours.

Discussion - In summary, we present a systematic and

generic VDMC approach for warm dense electron gas and obtain high-precision results for the LFC/XC kernel over a broad range of momentum and temperature. The VDMC allows for accurate and efficient calculation of various quantities directly in the thermodynamic limit at arbitrary temperature, beyond the reach of state-of-the-art path-integral-based MC methods. Our VDMC calculations have immediate practical applications in exploring various physical systems. For example, we obtain the first *ab initio* result for the real-space XC kernel, which enables finite- T TDDFT calculations for real electronic systems. A natural continuation of this work is to study the spin-dependent correlations and thermodynamic functions and construct the frequency-dependent LFC.

P.-C. Hou, B.-Z. Wang, and Y. Deng were supported by the National Natural Science Foundation of China (under Grant No. 11625522), the Innovation Program for Quantum Science and Technology (under grant no. 2021ZD0301900), and the National Key R&D Program of China (under Grants No. 2018YFA0306501). K. Chen and K. Haule were supported by the Simons Collaboration on the Many Electron Problem, and K. Haule was supported by NSF DMR-1709229.

* kunchen@flatironinstitute.org

- [1] D. Saumon and T. Guillot, *The Astrophysical Journal* **609**, 1170 (2004), ISSN 0004-637X, publisher: IOP Publishing, URL <https://iopscience.iop.org/article/10.1086/421257/meta>.
- [2] J. Vorberger, I. Tamblyn, B. Militzer, and S. A. Bonev, *Physical Review B* **75**, 024206 (2007), publisher: American Physical Society, URL <https://link.aps.org/doi/10.1103/PhysRevB.75.024206>.
- [3] N. Nettelmann, B. Holst, A. Kietzmann, M. French, R. Redmer, and D. Blaschke, *The Astrophysical Journal* **683**, 1217 (2008), ISSN 0004-637X, publisher: IOP Publishing, URL <https://iopscience.iop.org/article/10.1086/589806/meta>.
- [4] B. Militzer, W. B. Hubbard, J. Vorberger, I. Tamblyn, and S. A. Bonev, *The Astrophysical Journal* **688**, L45 (2008), ISSN 0004-637X, publisher: IOP Publishing, URL <https://iopscience.iop.org/article/10.1086/594364/meta>.
- [5] M. Schöttler and R. Redmer, *Physical Review Letters* **120**, 115703 (2018), publisher: American Physical Society, URL <https://link.aps.org/doi/10.1103/PhysRevLett.120.115703>.
- [6] D. Saumon, W. B. Hubbard, G. Chabrier, and H. M. van Horn, *The Astrophysical Journal* **391**, 827 (1992), ISSN 0004-637X, aDS Bibcode: 1992ApJ...391..827S, URL <https://ui.adsabs.harvard.edu/abs/1992ApJ...391..827S>.
- [7] A. Becker, W. Lorenzen, J. J. Fortney, N. Nettelmann, M. Schöttler, and R. Redmer, *The Astrophysical Journal Supplement Series* **215**, 21 (2014), ISSN 0067-0049, publisher: American Astronomical Society, URL <https://doi.org/10.1088/0067-0049/215/2/21>.
- [8] J. Daligault and S. Gupta, *The Astrophysical Journal* **703**, 994 (2009), ISSN 0004-637X, publisher: American Astronomical Society, URL <https://doi.org/10.1088/0004-637x/703/1/994>.
- [9] U. Zastrau, P. Sperling, M. Harmand, A. Becker, T. Bornath, R. Bredow, S. Dziarzhytski, T. Fennel, L. B. Fletcher, E. Förster, et al., *Phys. Rev. Lett.* **112**, 105002 (2014), URL <https://link.aps.org/doi/10.1103/PhysRevLett.112.105002>.
- [10] L. B. Fletcher, H. J. Lee, T. Döppner, E. Galtier, B. Nagler, P. Heimann, C. Fortmann, S. LePape, T. Ma, M. Millot, et al., *Nature Photonics* **9**, 274 (2015), ISSN 1749-4893, URL <https://www.nature.com/articles/nphoton.2015.41>.
- [11] P. Sperling, E. J. Gamboa, H. J. Lee, H. K. Chung, E. Galtier, Y. Omarbakiyeva, H. Reinholz, G. Röpke, U. Zastrau, J. Hastings, et al., *Phys. Rev. Lett.* **115**, 115001 (2015), URL <https://link.aps.org/doi/10.1103/PhysRevLett.115.115001>.
- [12] T. Tschentscher, C. Bressler, J. Grünert, A. Madsen, A. P. Mancuso, M. Meyer, A. Scherz, H. Sinn, and U. Zastrau, *Applied Sciences* **7**, 592 (2017), number: 6 Publisher: Multidisciplinary Digital Publishing Institute, URL <https://www.mdpi.com/2076-3417/7/6/592>.
- [13] E. Wigner, *Physical Review* **46**, 1002 (1934), ISSN 0031-899X, URL <https://link.aps.org/doi/10.1103/PhysRev.46.1002>.
- [14] E. Wigner, *Transactions of the Faraday Society* **34**, 678 (1938).
- [15] N. D. Drummond, Z. Radnai, J. R. Trail, M. D. Towler, and R. J. Needs, *Physical Review B* **69**, 085116 (2004), ISSN 1098-0121, 1550-235X, URL <https://link.aps.org/doi/10.1103/PhysRevB.69.085116>.
- [16] S. H. Glenzer and R. Redmer, *Reviews of Modern Physics* **81**, 1625 (2009), ISSN 0034-6861, 1539-0756, URL <https://link.aps.org/doi/10.1103/RevModPhys.81.1625>.
- [17] A. D. Baczewski, L. Shulenburger, M. P. Desjarlais, S. B. Hansen, and R. J. Magyar, *Physical Review Letters* **116**, 115004 (2016), ISSN 0031-9007, 1079-7114, URL <https://link.aps.org/doi/10.1103/PhysRevLett.116.115004>.
- [18] D. Kraus, B. Bachmann, B. Barbrel, R. W. Falcone, L. B. Fletcher, S. Frydrych, E. J. Gamboa, M. Gauthier, D. O. Gericke, S. H. Glenzer, et al., **61**, 014015 (2018), URL <https://doi.org/10.1088/1361-6587/aadd6c>.
- [19] T. G. White, J. Vorberger, C. R. D. Brown, B. J. B. Crowley, P. Davis, S. H. Glenzer, J. W. O. Harris, D. C. Hochhaus, S. Le Pape, T. Ma, et al., *Scientific Reports* **2**, 889 (2012), ISSN 2045-2322, URL <https://www.nature.com/articles/srep00889>.
- [20] A. Denoeud, N. Ozaki, A. Benuzzi-Mounaix, H. Uranishi, Y. Kondo, R. Kodama, E. Brambrink, A. Ravasio, M. Bocoum, J.-M. Boudenne, et al., *Proceedings of the National Academy of Sciences* **113** (2016), ISSN 0027-8424, 1091-6490, URL <https://www.pnas.org/content/113/28/7745>.
- [21] N. Medvedev and B. Ziaja, *Scientific Reports* **8** (2018), ISSN 2045-2322, URL <https://www.nature.com/articles/s41598-018-23632-8>.
- [22] T. Olsen, C. E. Patrick, J. E. Bates, A. Ruzsinszky, and K. S. Thygesen, *npj Computational Materials* **5**, 106 (2019), ISSN 2057-3960, URL <http://www.nature.com/>

- articles/s41524-019-0242-8.
- [23] S. H. Glenzer, O. L. Landen, P. Neumayer, R. W. Lee, K. Widmann, S. W. Pollaine, R. J. Wallace, G. Gregori, A. Höll, T. Bornath, et al., *Phys. Rev. Lett.* **98**, 065002 (2007), URL <https://link.aps.org/doi/10.1103/PhysRevLett.98.065002>.
- [24] S. M. Badalyan, C. S. Kim, and G. Vignale, *Physical Review Letters* **100**, 016603 (2008), publisher: American Physical Society, URL <https://link.aps.org/doi/10.1103/PhysRevLett.100.016603>.
- [25] S. K. Upadhyay and L. Saini, *Physica B: Condensed Matter* **614**, 412982 (2021), ISSN 09214526, URL <https://linkinghub.elsevier.com/retrieve/pii/S0921452621001812>.
- [26] M. P. Desjarlais, C. R. Scullard, L. X. Benedict, H. D. Whitley, and R. Redmer, *Physical Review E* **95**, 033203 (2017), publisher: American Physical Society, URL <https://link.aps.org/doi/10.1103/PhysRevE.95.033203>.
- [27] M. Veysman, G. Röpke, M. Winkel, and H. Reinholz, *Physical Review E* **94**, 013203 (2016), publisher: American Physical Society, URL <https://link.aps.org/doi/10.1103/PhysRevE.94.013203>.
- [28] W. Cayzac, A. Frank, A. Ortner, V. Bagnoud, M. M. Basko, S. Bedacht, C. Bläser, A. Blažević, S. Busold, O. Deppert, et al., *Nature Communications* **8**, 15693 (2017), ISSN 2041-1723, URL <https://www.nature.com/articles/ncomms15693>.
- [29] Z.-G. Fu, Z. Wang, and P. Zhang, *Physics of Plasmas* **24**, 112710 (2017), ISSN 1070-664X, publisher: American Institute of Physics, URL <https://aip.scitation.org/doi/10.1063/1.5008581>.
- [30] J. Vorberger, D. O. Gericke, T. Bornath, and M. Schlanges, *Phys. Rev. E* **81**, 046404 (2010), URL <https://link.aps.org/doi/10.1103/PhysRevE.81.046404>.
- [31] E. Runge and E. K. U. Gross, *Physical Review Letters* **52**, 997 (1984), ISSN 0031-9007, URL <https://link.aps.org/doi/10.1103/PhysRevLett.52.997>.
- [32] C. Ullrich, *Time-dependent density-functional theory: concepts and applications*, Oxford graduate texts (Oxford University Press, Oxford ; New York, 2012), ISBN 978-0-19-956302-9, oCLC: ocn751833811.
- [33] E. K. U. Gross and W. Kohn, *Physical Review Letters* **55**, 2850 (1985), ISSN 0031-9007, URL <https://link.aps.org/doi/10.1103/PhysRevLett.55.2850>.
- [34] N. Iwamoto and E. K. U. Gross, *Physical Review B* **35**, 3003 (1987), ISSN 0163-1829, URL <https://link.aps.org/doi/10.1103/PhysRevB.35.3003>.
- [35] A. Holas, in *Strongly Coupled Plasma Physics*, edited by F. J. Rogers and H. E. Dewitt (Springer US, Boston, MA, 1987), pp. 463–482, ISBN 978-1-4612-9053-7 978-1-4613-1891-0, URL http://link.springer.com/10.1007/978-1-4613-1891-0_41.
- [36] G. Vignale, *Physical Review B* **38**, 6445 (1988), ISSN 0163-1829, URL <https://link.aps.org/doi/10.1103/PhysRevB.38.6445>.
- [37] C. Bowen, G. Sugiyama, and B. J. Alder, *Physical Review B* **50**, 14838 (1994), ISSN 0163-1829, 1095-3795, URL <https://link.aps.org/doi/10.1103/PhysRevB.50.14838>.
- [38] S. Moroni, D. M. Ceperley, and G. Senatore, *Physical Review Letters* **75**, 689 (1995), ISSN 0031-9007, 1079-7114, URL <https://link.aps.org/doi/10.1103/PhysRevLett.75.689>.
- [39] K. Chen and K. Haule, *Nature Communications* **10**, 3725 (2019), ISSN 2041-1723, URL <http://www.nature.com/articles/s41467-019-11708-6>.
- [40] C. A. Kukkonen and K. Chen, *Physical Review B* **104**, 195142 (2021), ISSN 2469-9950, 2469-9969, URL <https://link.aps.org/doi/10.1103/PhysRevB.104.195142>.
- [41] J. P. F. LeBlanc, K. Chen, K. Haule, N. V. Prokof'ev, and I. S. Tupitsyn, *Dynamic response of the electron gas: Towards the exact exchange-correlation kernel* (2022), arXiv:2205.13595 [cond-mat], URL <http://arxiv.org/abs/2205.13595>.
- [42] T. Dornheim, S. Groth, A. Filinov, and M. Bonitz, *New J. Phys.* **17**, 073017 (2015), URL <http://dx.doi.org/10.1088/1367-2630/17/7/073017>.
- [43] T. Dornheim, T. Schoof, S. Groth, A. Filinov, and M. Bonitz, *The Journal of Chemical Physics* **143**, 204101 (2015), URL <https://doi.org/10.1063/1.4936145>.
- [44] T. Schoof, S. Groth, J. Vorberger, and M. Bonitz, *Phys. Rev. Lett.* **115**, 130402 (2015), URL <https://link.aps.org/doi/10.1103/PhysRevLett.115.130402>.
- [45] S. Groth, T. Schoof, T. Dornheim, and M. Bonitz, *Phys. Rev. B* **93**, 085102 (2016), URL <https://link.aps.org/doi/10.1103/PhysRevB.93.085102>.
- [46] T. Dornheim, J. Vorberger, S. Groth, N. Hoffmann, Z. A. Moldabekov, and M. Bonitz, *The Journal of Chemical Physics* **151**, 194104 (2019), ISSN 0021-9606, 1089-7690, URL <http://aip.scitation.org/doi/10.1063/1.5123013>.
- [47] M. Corradini, R. Del Sole, G. Onida, and M. Palumbo, *Physical Review B* **57**, 14569 (1998), ISSN 0163-1829, 1095-3795, URL <https://link.aps.org/doi/10.1103/PhysRevB.57.14569>.
- [48] T. Dornheim, A. Cangi, K. Ramakrishna, M. Böhme, S. Tanaka, and J. Vorberger, *Physical Review Letters* **125**, 235001 (2020), ISSN 0031-9007, 1079-7114, URL <https://link.aps.org/doi/10.1103/PhysRevLett.125.235001>.
- [49] T. Dornheim, Z. A. Moldabekov, and P. Tolias, *Physical Review B* **103**, 165102 (2021), ISSN 2469-9950, 2469-9969, URL <https://link.aps.org/doi/10.1103/PhysRevB.103.165102>.
- [50] T. Dornheim, M. Böhme, Z. A. Moldabekov, J. Vorberger, and M. Bonitz, *Physical Review Research* **3**, 033231 (2021), ISSN 2643-1564, URL <https://link.aps.org/doi/10.1103/PhysRevResearch.3.033231>.
- [51] G. Giuliani and G. Vignale, *Quantum Theory of the Electron Liquid* (Cambridge University Press, 2005).
- [52] M. Troyer and U.-J. Wiese, *Physical Review Letters* **94**, 170201 (2005), ISSN 0031-9007, 1079-7114, URL <https://link.aps.org/doi/10.1103/PhysRevLett.94.170201>.
- [53] T. Dornheim, S. Groth, A. V. Filinov, and M. Bonitz, *The Journal of Chemical Physics* **151**, 014108 (2019), ISSN 0021-9606, publisher: American Institute of Physics, URL <https://aip.scitation.org/doi/10.1063/1.5093171>.
- [54] T. Dornheim, *Physical Review E* **100**, 023307 (2019), ISSN 2470-0045, 2470-0053, URL <https://link.aps.org/doi/10.1103/PhysRevE.100.023307>.
- [55] T. Dornheim, S. Groth, and M. Bonitz, *Physics Reports* **744**, 1 (2018), ISSN 03701573, URL <https://linkinghub.elsevier.com/retrieve/pii/S0370157318300516>.

- [56] S. Groth, T. Dornheim, T. Sjoström, F. D. Malone, W. M. C. Foulkes, and M. Bonitz, *Physical Review Letters* **119**, 135001 (2017), ISSN 0031-9007, 1079-7114, URL <https://link.aps.org/doi/10.1103/PhysRevLett.119.135001>.
- [57] W. D. Kraeft, M. Schlanges, J. Vorberger, and H. E. DeWitt, *Physical Review E* **66**, 046405 (2002), ISSN 1063-651X, 1095-3787, URL <https://link.aps.org/doi/10.1103/PhysRevE.66.046405>.
- [58] S. Groth, T. Dornheim, and J. Vorberger, *Physical Review B* **99**, 235122 (2019), ISSN 2469-9950, 2469-9969, URL <https://link.aps.org/doi/10.1103/PhysRevB.99.235122>.
- [59] D. J. W. Geldart and R. Taylor, *Canadian Journal of Physics* **48**, 167 (1970), ISSN 0008-4204, 1208-6045, URL <http://www.nrcresearchpress.com/doi/10.1139/p70-023>.
- [60] F. Broens, J. T. Devreese, and L. F. Lemmens, *Physical Review B* **21**, 1363 (1980), ISSN 0163-1829, URL <https://link.aps.org/doi/10.1103/PhysRevB.21.1363>.
- [61] B. Farid, V. Heine, G. E. Engel, and I. J. Robertson, *Physical Review B* **48**, 11602 (1993), ISSN 0163-1829, 1095-3795, URL <https://link.aps.org/doi/10.1103/PhysRevB.48.11602>.
- [62] C. F. Richardson and N. W. Ashcroft, *Physical Review B* **50**, 8170 (1994), ISSN 0163-1829, 1095-3795, URL <https://link.aps.org/doi/10.1103/PhysRevB.50.8170>.
- [63] P. A. Martin, *Reviews of Modern Physics* **60**, 1075 (1988), ISSN 0034-6861, URL <https://link.aps.org/doi/10.1103/RevModPhys.60.1075>.
- [64] See Supplemental Material for additional information.
- [65] B. Militzer and E. L. Pollock, *Physical Review Letters* **89**, 280401 (2002), ISSN 0031-9007, 1079-7114, URL <https://link.aps.org/doi/10.1103/PhysRevLett.89.280401>.
- [66] K. Hunger, T. Schoof, T. Dornheim, M. Bonitz, and A. Filinov, *Physical Review E* **103**, 053204 (2021), ISSN 2470-0045, 2470-0053, URL <https://link.aps.org/doi/10.1103/PhysRevE.103.053204>.
- [67] N. V. Prokof'ev and B. V. Svistunov, *Phys. Rev. Lett.* **81**, 2514 (1998).
- [68] E. Kozik, K. V. Houcke, E. Gull, L. Pollet, N. V. Prokof'ev, B. V. Svistunov, and M. Troyer, *EPL* **90**, 10004 (2010).
- [69] J. Gukelberger, E. Kozik, L. Pollet, N. V. Prokof'ev, M. Sgrist, B. V. Svistunov, and M. Troyer, *Phys. Rev. Lett.* **113**, 195301 (2014).
- [70] Y. Deng, E. Kozik, N. V. Prokof'ev, and B. V. Svistunov, *EPL* **110**, 57001 (2015).
- [71] W. Wu, M. Ferrero, A. Georges, and E. Kozik, *Phys. Rev. B* **96**, 041105(R) (2017), URL <https://link.aps.org/doi/10.1103/PhysRevB.96.041105>.
- [72] F. Šimković, Y. Deng, N. V. Prokof'ev, B. V. Svistunov, I. S. Tupitsyn, and E. Kozik, *Phys. Rev. B* **96**, 081117(R) (2017), URL <https://link.aps.org/doi/10.1103/PhysRevB.96.081117>.
- [73] A. Moutenet, W. Wu, and M. Ferrero, *Phys. Rev. B* **97**, 085117 (2018).
- [74] A. Taheridehkordi, S. H. Curnoe, and J. P. F. LeBlanc, *Phys. Rev. B* **99**, 035120 (2019).
- [75] F. Šimković and E. Kozik, *Phys. Rev. B* **100**, 121102(R) (2019), URL <https://link.aps.org/doi/10.1103/PhysRevB.100.121102>.
- [76] J. Vučićević and M. Ferrero, *Phys. Rev. B* **101**, 075113 (2020), URL <https://link.aps.org/doi/10.1103/PhysRevB.101.075113>.
- [77] A. J. Kim, F. Šimković, and E. Kozik, *Phys. Rev. Lett.* **124**, 117602 (2020).
- [78] K. Van Houcke, F. Werner, E. Kozik, N. V. Prokof'ev, B. V. Svistunov, M. Ku, A. Sommer, L. Cheuk, A. Schirrotzek, and M. Zwierlein, *Nature Physics* **8**, 366 (2012).
- [79] K. Van Houcke, F. Werner, T. Ohgoe, N. V. Prokof'ev, and B. V. Svistunov, *Phys. Rev. B* **99**, 035140 (2019).
- [80] R. Rossi, T. Ohgoe, K. Van Houcke, and F. Werner, *Phys. Rev. Lett.* **121**, 130405 (2018).
- [81] R. Rossi, T. Ohgoe, E. Kozik, N. V. Prokof'ev, B. V. Svistunov, K. Van Houcke, and F. Werner, *Phys. Rev. Lett.* **121**, 130406 (2018).
- [82] A. S. Mishchenko, N. V. Prokof'ev, A. Sakamoto, and B. V. Svistunov, *Phys. Rev. B* **62**, 6317 (2000).
- [83] N. Prokof'ev and B. Svistunov, *Phys. Rev. B* **77**, 020408(R) (2008).
- [84] N. V. Prokof'ev and B. V. Svistunov, *Phys. Rev. B* **77**, 125101 (2008).
- [85] P. Kroiss and L. Pollet, *Phys. Rev. B* **90**, 104510 (2014).
- [86] A. S. Mishchenko, N. Nagaosa, and N. V. Prokof'ev, *Phys. Rev. Lett.* **113**, 166402 (2014).
- [87] T. Hahn, S. Klimin, J. Tempere, J. T. Devreese, and C. Franchini, *Phys. Rev. B* **97**, 134305 (2018).
- [88] A. S. Mishchenko, L. Pollet, N. V. Prokof'ev, A. Kumar, D. L. Maslov, and N. Nagaosa, *Phys. Rev. Lett.* **123**, 076601 (2019).
- [89] K. Van Houcke, F. Werner, and R. Rossi, *Phys. Rev. B* **101**, 045134 (2020).
- [90] S. A. Kulagin, N. V. Prokof'ev, O. A. Starykh, B. V. Svistunov, and C. N. Varney, *Phys. Rev. Lett.* **110**, 070601 (2013).
- [91] S. A. Kulagin, N. V. Prokof'ev, O. A. Starykh, B. V. Svistunov, and C. N. Varney, *Phys. Rev. B* **87**, 024407 (2013).
- [92] Y. Huang, K. Chen, Y. Deng, N. V. Prokof'ev, and B. V. Svistunov, *Phys. Rev. Lett.* **116**, 177203 (2016).
- [93] K. Haule and K. Chen, *Scientific Reports* **12**, 2294 (2022), ISSN 2045-2322, URL <https://www.nature.com/articles/s41598-022-06188-6>.
- [94] H. Kleinert, *Path Integrals in Quantum Mechanics, Statistics, and Polymer Physics* (WORLD SCIENTIFIC, 1995), 2nd ed., ISBN 978-981-02-1471-5 978-981-4535-51-9, URL <http://www.worldscientific.com/worldscibooks/10.1142/2092>.
- [95] B.-Z. Wang, P.-C. Hou, Y. Deng, K. Haule, and K. Chen, *Physical Review B* **103**, 115141 (2021), ISSN 2469-9950, 2469-9969, URL <https://link.aps.org/doi/10.1103/PhysRevB.103.115141>.
- [96] S. Tanaka and S. Ichimaru, *Journal of the Physical Society of Japan* **55**, 2278 (1986), ISSN 0031-9015, 1347-4073, URL <http://journals.jps.jp/doi/10.1143/JPSJ.55.2278>.

Supplemental Material: Exchange-Correlation Effect in the Charge Response of a Warm Dense Electron Gas

Peng-Cheng Hou¹, Bao-Zong Wang¹, Kristjan Haule⁴, Youjin Deng^{1,2,3}, and Kun Chen^{5*}

¹ Department of Modern Physics, University of Science and Technology of China, Hefei, Anhui 230026, China

² Hefei National Laboratory, University of Science and Technology of China, Hefei 230088, China

³ MinJiang Collaborative Center for Theoretical Physics,

College of Physics and Electronic Information Engineering, Minjiang University, Fuzhou 350108, China

⁴ Department of Physics and Astronomy, Rutgers,

The State University of New Jersey, Piscataway, New Jersey 08854-8019 USA and

⁵ Center for Computational Quantum Physics, Flatiron Institute, 162 5th Avenue, New York, New York 10010. The Flatiron Institute is a division of the Simons Foundation

DERIVATION OF THE ASYMPTOTIC FORMULA OF THE STATIC EXCHANGE-CORRELATION KERNEL IN LARGE-MOMENTUM LIMIT

The dynamic exchange-correlation (XC) kernel $K_{xc}(q, i\nu_m)$ ($\nu_m = 2m\pi/\beta$ is the bosonic Matsubara frequency) is defined as

$$K_{xc}(q, i\nu_m) = \frac{1}{\chi_0(q, i\nu_m)} - \frac{1}{\Pi(q, i\nu_m)}, \quad (S1)$$

where Π is the polarization function and the noninteracting density response function χ_0 is actually the zero-order diagram in Π . Here, we develop the large- q expansion of $\Pi(\mathbf{q}, i\nu_m)$ with finite ν_m and derive the asymptotic expression of the static XC kernel $K_{xc}(q)$ in the large- q limit.

We first formulate the perturbative expansion for $\Pi(q, i\nu_m)$ by Hedin's equations. As shown in Fig. S1(a), each contribution of Π is computed by multiplying the amplitudes, including bare propagator \mathcal{G}_0 , bold propagator \mathcal{G} , effective potential W , self-energy Σ , and vertex function Γ . Expanding \mathcal{G}_0 with flowing external momentum q as

$$\begin{aligned} \mathcal{G}_0(\mathbf{k} + \mathbf{q}, i\omega_n + i\nu_m) &= \frac{1}{i\omega_n + i\nu_m - (\mathbf{k} + \mathbf{q})^2 + \mu} \\ &= \frac{-1}{q^2} - \frac{\mathcal{G}_0^{-1}(\mathbf{k}, i\omega_n) - 2\mathbf{k} \cdot \mathbf{q} + 4(\mathbf{k} \cdot \hat{\mathbf{q}})^2 + i\nu_m}{q^4} + O(q^{-6}), \end{aligned} \quad (S2)$$

where $\omega_n = (2n + 1)\pi/\beta$ is the fermionic Matsubara frequency and μ is the chemical potential, we find that each bare propagator \mathcal{G}_0 with flowing q contributes $-1/q^2$ and the subleading $1/q^4$ terms for Π . Therefore, we can determine the dominant large- q contribution of each polarization diagram as $\sim 1/q^{2\ell}$, where ℓ is the least number of the propagator lines with flowing q . As shown in the second line of Fig. S1(a), we give all polarization diagrams with $\ell = 1$ or 2, including the zero-order diagram χ_0 , the high-order diagrams having self-energy in insertion without vertex corrections, and the high-order diagrams with only one vertex correction.

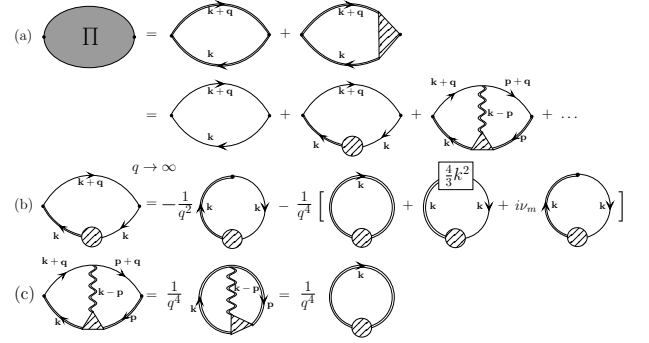


FIG. S1. (a) The perturbative expansion for the polarization function $\Pi(\mathbf{q}, i\nu_m)$ formulated with the standard Feynman diagrams. The diagrams plotted in the second line include all diagrams whose leading term is proportional to $1/q^2$ or $1/q^4$ in the large- q expansion of Π . The solid and double lines represent the bare propagator \mathcal{G}_0 and the bold propagator \mathcal{G} , respectively. The double wave represents the effective potential W , the shaded circle represents the self-energy Σ , and the shaded triangular represents the one-interaction-irreducible vertex function Γ . (b) The large- q expansion up to $1/q^4$ for the high-order diagrams having self-energy insertion without vertex corrections. The $1/q^2$ term and the last $1/q^4$ term with prefactor $i\nu_m$ equal zero according to Dyson's equation and the density conservation. The second $1/q^4$ term equals $8/3$ times the interaction-induced shift of the kinetic energy δE_k . (c) The large- q expansion up to $1/q^4$ for the high-order diagrams with one vertex correction. It cancels with the first $1/q^4$ term in (b). The second equation is given by Hedin's equations.

We next present the derivation of the large- q expansion of χ_0 for any finite Matsubara frequency ν_m , which reads

$$\begin{aligned} \chi_0(q, i\nu_m) &= -\frac{2}{\beta} \int d\mathbf{k} \sum_n \mathcal{G}_0(\mathbf{k}, i\omega_n) \mathcal{G}_0(\mathbf{k} + \mathbf{q}, i\omega_n + i\nu_m) \\ &= -2 \int d\mathbf{k} \frac{f(\epsilon_{\mathbf{k}}) - f(\epsilon_{\mathbf{k}+\mathbf{q}})}{i\nu_m + \epsilon_{\mathbf{k}} - \epsilon_{\mathbf{k}+\mathbf{q}}} \\ &= \int_0^\infty \frac{dk}{(2\pi)^2} \frac{k}{q} f(\epsilon_{\mathbf{k}}) \ln \frac{\nu_m^2 + (q^2 + 2kq)^2}{\nu_m^2 + (q^2 - 2kq)^2}, \end{aligned} \quad (S3)$$

where the factor 2 comes from spin summation and $f(\epsilon_{\mathbf{k}}) = \sum_n \mathcal{G}_0(\mathbf{k}, i\omega_n) e^{i\omega_n 0^+}$ is the momentum distribu-

tion of noninteracting fermions. Expanding the integrand for $q \rightarrow \infty$, we obtain

$$\begin{aligned}\chi_0(q, i\nu_m) &= 8 \int \frac{dk}{(2\pi)^2} k^2 f(\epsilon_{\mathbf{k}}) \left[\frac{1}{q^2} + \frac{4k^2}{3q^4} + \mathcal{O}(q^{-6}) \right] \\ &= \frac{2\rho}{q^2} + \frac{8}{3} \frac{E_{k0}}{q^4} + \mathcal{O}(q^{-6}).\end{aligned}\quad (\text{S4})$$

Here, density $\rho \equiv (4\pi r_s^3/3)^{-1}$ is equal to $2 \int d\mathbf{k} f(\epsilon_{\mathbf{k}})$ and the noninteracting kinetic energy E_{k0} is equal to $2 \int d\mathbf{k} k^2 f(\epsilon_{\mathbf{k}})$. Moreover, the large- q expansion of χ_0 can also be directly derived using the \mathcal{G}_0 expansion in Eq.(S2).

We now turn to the large- q expansion of the high-order diagrams up to $1/q^4$. For the diagrams in Fig. S1(b), the $1/q^2$ -term $\int d\mathbf{k} \sum_n \mathcal{G} \Sigma \mathcal{G}_0(\mathbf{k}, i\omega_n)$ can be rewritten as $\int d\mathbf{k} \sum_n [\mathcal{G} - \mathcal{G}_0](\mathbf{k}, i\omega_n)$ via Dyson's equation, which vanishes due to the density conservation. The $1/q^4$ terms have three parts: the first one comes from the \mathcal{G}_0^{-1}/q^4 contribution in Eq.(S2); the second one is obtained after integrating the angle in $4(\mathbf{k} \cdot \hat{\mathbf{q}})^2/q^4$ as

$$\begin{aligned}& 2 \int d\mathbf{k} \frac{4(\mathbf{k} \cdot \hat{\mathbf{q}})^2}{q^4} \sum_n \mathcal{G} \Sigma \mathcal{G}_0(\mathbf{k}, i\omega_n) \\ &= 2 \int_0^\infty \frac{dk}{(2\pi)^2} \int_{-1}^1 d\cos\theta \frac{4k^4 \cos^2\theta}{q^4} \sum_n \mathcal{G} \Sigma \mathcal{G}_0(k, i\omega_n) \\ &= 2 \int d\mathbf{k} \frac{4k^2}{3q^4} \sum_n \mathcal{G} \Sigma \mathcal{G}_0(k, i\omega_n),\end{aligned}\quad (\text{S5})$$

where the factor 2 comes from spin summation; and the third one comes from the $i\nu_m/q^4$ contribution in Eq. (S2), which vanishes like the $1/q^2$ term. Similarly, we obtain the $1/q^4$ term of the diagrams with one vertex correction in Fig. S1(c), which exactly cancels the first $1/q^4$ term in Fig. S1(b). Consequently, the only existed term is the $1/q^4$ term in Eq. (S5). Finally, we obtain the large- q expansion of high-order polarization as

$$\begin{aligned}& \lim_{q \rightarrow \infty} [\Pi - \chi_0](q, i\nu_m) \\ &= 2 \int d\mathbf{k} \frac{8k^2}{3q^4} \sum_n \mathcal{G} \Sigma \mathcal{G}_0(\mathbf{k}, i\omega_n) + \mathcal{O}(q^{-6}) \\ &= \frac{16}{3q^4} \int d\mathbf{k} k^2 \sum_n \mathcal{G}(\mathbf{k}, i\omega_n) - \mathcal{G}_0(\mathbf{k}, i\omega_n) + \mathcal{O}(q^{-6}) \\ &= \frac{8}{3q^4} (E_{\mathbf{k}} - E_{k0}) + \mathcal{O}(q^{-6}),\end{aligned}\quad (\text{S6})$$

where the factor 2 is the symmetry factor. Interestingly, the coefficient of the $1/q^4$ term is exactly 8/3 times the interaction-induced shift of the kinetic energy $\delta E_{\mathbf{k}} \equiv E_{\mathbf{k}} - E_{k0}$. It is noted that the leading-order term does not depend on ν_m , which should exist on high-order terms.

Substituting Eq.(S4) and Eq.(S6) into Eq.(S1), we obtain the asymptotic formula of $K_{xc}(q)$ in the large- q limit

θ	E_{k0}	$E_{\mathbf{k}}$	$\delta E_{\mathbf{k}}$
0.0625	0.536 000	0.552 14(142)	0.016 14
0.25	0.647 785	0.653 23(236)	0.005 45
0.4	0.790 910	0.789 27(197)	-0.001 64
0.5	0.898 322	0.891 78(188)	-0.006 54
1	1.491 929	1.473 95(200)	-0.017 98
2	2.761 287	2.742 35(34)	-0.018 94
4	5.363 294	5.349 57(20)	-0.013 72
6	7.985 161	7.974 66(20)	-0.010 50
8	10.613 473	10.605 81(37)	-0.007 66
12	15.877 866	15.871 72(17)	-0.006 15
16	21.146 840	21.141 95(18)	-0.004 89

TABLE I. Kinetic energies $E_{\mathbf{k}}$ from VDMC simulations and ideal kinetic energies E_{k0} from numerical integration (errors can be neglected compared to $E_{\mathbf{k}}$'s) for $r_s = 1$.

as

$$\begin{aligned}\lim_{q \rightarrow \infty} K_{xc}(q; r_s, T) &= -\frac{2}{3\rho^2} \delta E_{\mathbf{k}}(r_s, T) + \mathcal{O}(q^{-2}) \\ &= -\frac{32\pi^2 r_s^6}{27} \delta E_{\mathbf{k}}(r_s, T) + \mathcal{O}(q^{-2}).\end{aligned}\quad (\text{S7})$$

This formula holds for the dynamic XC kernel with any finite frequency since the frequency dependence does not exist in the leading order.

CALCULATION OF THE KINETIC ENERGY

The kinetic energy of the three-dimensional uniform electron gas reads

$$E_{\mathbf{k}} = 2 \int d\mathbf{k} k^2 \mathcal{G}(\mathbf{k}, \tau = 0^-), \quad (\text{S8})$$

where τ is imaginary time. By setting each component with q in the polarization diagrams $\mathcal{G}(\mathbf{k} + \mathbf{q}, \tau) \mathcal{G}(\mathbf{k}, -\tau)$ to one, all the diagrams of the bold propagator $\mathcal{G}(\mathbf{k}, \tau)$ are generated using the Feynman diagrammatic expansion for the polarization in the variational scheme [1]. Therefore, we can directly calculate $E_{\mathbf{k}}$ by the variational diagrammatic Monte Carlo (VDMC) method. Moreover, we calculate the noninteracting kinetic energy

$$\begin{aligned}E_{k0} &= 2 \int d\mathbf{k} k^2 \mathcal{G}_0(\mathbf{k}, \tau = 0^-) \\ &= \int dk \frac{k^4}{\pi^2} \frac{1}{e^{k^2 - \mu} + 1},\end{aligned}\quad (\text{S9})$$

by a one-dimensional numerical integration. All the data of $E_{\mathbf{k}}$ and E_{k0} are given in Tables I.

DATA TABLE OF THE LOCAL FIELD CORRECTION

All the local field correction data given in Tables II and III are obtained by performing VDMC simulations for

the truncation order $N = 5$ and including extrapolation errors.

TABLE II. Static local field corrections $G(q, \theta)$ for $r_s = 1$ from VDMC simulations.

θ	q/k_F	G	error
0.0625	0.1875	0.0090	0.0003
0.0625	0.3750	0.0359	0.0012
0.0625	0.5625	0.0814	0.0027
0.0625	0.7500	0.1463	0.0044
0.0625	0.9375	0.2329	0.0065
0.0625	1.1250	0.3448	0.0092
0.0625	1.3125	0.4867	0.0123
0.0625	1.5000	0.6609	0.0159
0.0625	1.6875	0.8715	0.0204
0.0625	1.8750	1.0805	0.0259
0.0625	2.0000	1.1175	0.0241
0.0625	2.2500	1.0295	0.0368
0.0625	2.5000	1.0190	0.0383
0.0625	2.7500	1.0270	0.0414
0.0625	3.0000	1.0318	0.0477
0.0625	3.5000	1.0520	0.0525
0.0625	4.0000	1.1068	0.0660
0.0625	4.5000	1.1931	0.0839
0.0625	5.0000	1.2956	0.1056
0.0625	5.5000	1.4231	0.1321
0.0625	6.0000	1.5537	0.1640
0.0625	6.5000	1.6908	0.1896
0.0625	7.0000	1.7712	0.3640
0.0625	8.0000	2.0620	0.4874
0.0625	9.0000	2.3935	0.5872
0.0625	10.0000	2.7799	0.7599
0.25	0.1875	0.0093	0.0003
0.25	0.3750	0.0372	0.0011
0.25	0.5625	0.0842	0.0021
0.25	0.7500	0.1515	0.0032
0.25	0.9375	0.2406	0.0045
0.25	1.1250	0.3537	0.0059
0.25	1.3125	0.4914	0.0074
0.25	1.5000	0.6510	0.0090
0.25	1.6875	0.8205	0.0111
0.25	1.8750	0.9710	0.0144
0.25	2.0625	1.0581	0.0181
0.25	2.2500	1.0599	0.0275
0.25	2.4375	1.0019	0.0409
0.25	2.6250	0.9356	0.0558
0.25	2.8125	0.9053	0.0731
0.25	3.0000	0.8317	0.0595
0.25	4.0000	0.8502	0.0800
0.25	5.0000	0.9103	0.1311
0.25	6.0000	1.0118	0.2118
0.25	7.0000	1.1298	0.3172
0.25	8.0000	1.2461	0.4547
0.4	0.2500	0.0176	0.0005
0.4	0.5000	0.0705	0.0015
0.4	0.7500	0.1597	0.0028
0.4	1.0000	0.2862	0.0042
0.4	1.2500	0.4497	0.0062
0.4	1.5000	0.6415	0.0080
0.4	1.7500	0.8389	0.0103
0.4	2.0000	0.9970	0.0130
0.4	2.2500	1.0589	0.0175
0.4	2.5000	1.0041	0.0272
0.4	2.7500	0.8297	0.0396
0.4	3.0000	0.6830	0.0428
0.4	3.2500	0.5817	0.0462
0.4	3.5000	0.5303	0.0503
0.4	3.7500	0.5106	0.0559
0.4	4.0000	0.4992	0.0622
0.4	4.5000	0.4808	0.0791
0.4	5.0000	0.4529	0.1021
0.4	5.5000	0.4190	0.1284
0.4	6.0000	0.3767	0.1529
0.4	6.5000	0.3386	0.1890
0.4	7.0000	0.3027	0.2293
0.4	7.5000	0.2442	0.2692
1	0.2500	0.0196	0.0004
1	0.5000	0.0766	0.0015
1	0.7500	0.1670	0.0031
1	1.0000	0.2849	0.0048
1	1.2500	0.4239	0.0061
1	1.5000	0.5762	0.0072
1	1.7500	0.7304	0.0071
1	2.0000	0.8732	0.0070
1	2.2500	0.9884	0.0055
1	2.5000	1.0570	0.0063
1	2.7500	1.0607	0.0045
1	3.0000	0.9884	0.0101
1	3.2500	0.8481	0.0107
1	3.5000	0.6317	0.0270
1	3.7500	0.3957	0.0302
1	4.0000	0.0936	0.0613
1	4.5000	-0.3062	0.0562
1	5.0000	-0.6051	0.1124
1	5.5000	-0.7602	0.0971
1	6.5000	-1.0423	0.1331
1	7.5000	-1.4262	0.1711
1	8.5000	-1.9074	0.2438
2	0.5000	0.0669	0.0025
2	1.0000	0.2343	0.0061
2	1.5000	0.4562	0.0078
2	2.0000	0.6968	0.0078
2	2.5000	0.9168	0.0076
2	3.0000	1.0654	0.0039
2	3.5000	1.0821	0.0039
2	4.0000	0.9199	0.0066
2	4.5000	0.5668	0.0125
2	5.0000	0.0631	0.0228
2	6.0000	-1.0253	0.0531

θ	q/k_F	G	error
2	7.0000	-1.7685	0.0918
2	8.0000	-2.2129	0.1404
2	9.0000	-2.6287	0.2060
4	0.3125	0.0197	0.0015
4	0.6250	0.0720	0.0044
4	0.9375	0.1452	0.0067
4	1.2500	0.2338	0.0081
4	1.5625	0.3297	0.0090
4	1.8750	0.4382	0.0096
4	2.1875	0.5505	0.0106
4	2.5000	0.6621	0.0070
4	2.8125	0.7729	0.0068
4	3.1250	0.8770	0.0065
4	3.4375	0.9690	0.0063
4	3.7500	1.0434	0.0062
4	4.0625	1.0941	0.0062
4	4.3750	1.1146	0.0064
4	4.6875	1.0996	0.0067
4	5.0000	1.0438	0.0106
4	6.0000	0.5620	0.0183
4	7.0000	-0.3278	0.0333
4	8.0000	-1.3619	0.0617
4	9.0000	-2.2441	0.1022
4	10.0000	-2.8511	0.1170
4	11.0000	-3.3196	0.2457
4	12.0000	-3.5672	0.3957
4	13.0000	-4.1618	0.4452
4	14.0000	-4.6946	0.4876
8	0.3125	0.0123	0.0013
8	0.6250	0.0443	0.0039
8	0.9375	0.0883	0.0059
8	1.2500	0.1404	0.0075
8	1.5625	0.1986	0.0090
8	1.8750	0.2639	0.0107
8	2.1875	0.3373	0.0121
8	2.5000	0.4082	0.0146
8	2.8125	0.4841	0.0174
8	3.1250	0.5677	0.0215
8	3.4375	0.6555	0.0248
8	3.7500	0.7297	0.0315
8	4.0625	0.7957	0.0397
8	4.3750	0.8760	0.0505
8	4.6875	0.9496	0.0637
8	5.0000	1.0204	0.0128
8	6.0000	1.1164	0.0176
8	7.0000	1.0156	0.0252
8	8.0000	0.6601	0.0436
8	9.0000	0.0443	0.0707
8	10.0000	-0.7639	0.1337
8	11.0000	-1.6473	0.2022
8	12.0000	-2.4692	0.3048

* kunchen@flatironinstitute.org

θ	q/k_F	G	error
4	0.5000	0.0537	0.0052
4	1.0000	0.1869	0.0138
4	1.5000	0.3577	0.0185
4	2.0000	0.5424	0.0190
4	2.5000	0.7277	0.0171
4	3.0000	0.9006	0.0143
4	3.5000	1.0460	0.0119
4	4.0000	1.1457	0.0103
4	4.5000	1.1808	0.0107
4	5.0000	1.1340	0.0131
4	5.5000	0.9928	0.0188
4	6.0000	0.7566	0.0274
4	6.5000	0.4359	0.0399
4	7.0000	0.0569	0.0557
4	7.5000	-0.3491	0.0720
4	8.0000	-0.7437	0.0987
4	8.5000	-1.1015	0.1266
4	9.0000	-1.4006	0.1485
4	9.5000	-1.6456	0.1853
4	10.0000	-1.8453	0.1878
4	10.5000	-2.0122	0.2696
4	11.0000	-2.1482	0.3101
4	11.5000	-2.3023	0.3541
8	0.5000	0.0349	0.0041
8	1.0000	0.1204	0.0106
8	1.5000	0.2293	0.0140
8	2.0000	0.3497	0.0147
8	2.5000	0.4774	0.0142
8	3.0000	0.6088	0.0134
8	3.5000	0.7397	0.0126
8	4.0000	0.8654	0.0122
8	4.5000	0.9789	0.0121
8	5.0000	1.0731	0.0122
8	5.5000	1.1398	0.0131
8	6.0000	1.1703	0.0144
8	6.5000	1.1573	0.0159
8	7.0000	1.0937	0.0183
8	7.5000	0.9738	0.0215
8	8.0000	0.7961	0.0291
8	8.5000	0.5616	0.0343
8	9.0000	0.2772	0.0536
8	9.5000	-0.0498	0.0514
8	10.0000	-0.4057	0.0524
8	10.5000	-0.7733	0.0865
8	11.0000	-1.1386	0.1455
8	11.5000	-1.4967	0.1431

TABLE III. Static local field corrections $G(q, \theta)$ for $r_s = 2$ from VDMC simulations.

- [1] K. Chen and K. Haule, Nature Communications **10**, 3725 (2019), ISSN 2041-1723, URL <http://www.nature.com/articles/s41467-019-11708-6>.